
# Experimental investigation of the heat transfer from the helical coil heat exchanger using bubble injection for cold thermal energy storage system

Downloaded from: https://research.chalmers.se, 2026-04-07 02:41 UTC

Citation for the original published paper (version of record):
Zarei, A., Seddighi, S., Elahi, S. et al (2022). Experimental investigation of the heat transfer from the helical coil heat exchanger using
bubble injection for cold thermal energy storage system. Applied Thermal Engineering, 200.
http://dx.doi.org/10.1016/j.applthermaleng.2021.117559

N.B. When citing this work, cite the original published paper.

research.chalmers.se offers the possibility of retrieving research publications produced at Chalmers University of Technology. It covers all kind of research output: articles, dissertations, conference papers, reports etc. since 2004. research.chalmers.se is administrated and maintained by Chalmers Library

(article starts on next page)

Applied Thermal Engineering 200 (2022) 117559

Contents lists available at ScienceDirect

Applied Thermal Engineering

journal homepage: www.elsevier.com/locate/apthermeng

# Experimental investigation of the heat transfer from the helical coil heat exchanger using bubble injection for cold thermal energy storage system

Ahmad Zarei [a], Sadegh Seddighi [a,b,*], Sohail Elahi [a], Ramis Örlü [c,*]

[a] Department of Mechanical Engineering, K. N. Toosi University of Technology, Tehran, Iran
[b] Division of Energy Technology, Chalmers University of Technology, Gothenburg, Sweden
[c] Linné FLOW Centre, KTH Mechanics, SE-100 44 Stockholm, Sweden

ARTICLE INFO

*Keyword:*
Energy storages
Helical coils
Air bubble injection
Nusselt number
*COP* improvement

ABSTRACT

This study investigates cold thermal energy storage (*CTES*) using a helical coil heat exchanger modified with bubble injection. One of the effective methods for increasing the heat transfer rate in heat exchangers is using bubble injection. A helical coil heat exchanger is immersed inside a cylindrical water storage tank, where the helical coil is the evaporator of a vapor compression refrigeration cycle (*VCRC*) and provides the designed cooling. Experimental studies were carried out to examine the impact of bubble injection on Nusselt number, the temperature differences in the storage tank, exergy degradation in the evaporator, and cycle coefficient of performance (*COP*). The bubbles were injected from the bottom of the storage tank in four different geometries at airflow rates ranging from 3 to 11 L/min. The experimental results of this study revealed that bubble injection could significantly increase the COP and heat transfer rate from the storage tank, as well as the exergy destruction and Nusselt number (*Nu*). This increase was highly dependent on the geometry and flow rate of the bubble injection. The results also indicated that the bubble injection has an optimal flow rate value, which was 9 L/min in this study. More specifically, the *COP* of the refrigeration cycle and the *Nu* number increased by 124% and 452%, respectively, compared to the non-bubble injection mode. Finally, for calculating the outside Nusselt number of the helical coil, an empirical correlation as a function of bubble flow rate and bubble injection angle was proposed.

## 1. Introduction

Energy storage is an important component of modern energy systems and is being pursued in a variety of applications such as food storage and air conditioning systems [1]. Cold thermal energy storage (CTES) in energy systems is one method for reducing peak energy consumption [2]. CTES technology can be implemented using an electric refrigerator. Generally, cold thermal energy storage (CTES) is far less expensive than saving electricity for cold production [3]. The following benefits are associated with the use of cold storage technology: a) essential role in "peak load shifting", b) lowering the cooling system's energy consumption, c) lowering the system's operating costs during peak hours, and d) reducing the environmental pollution [1,2].

Increasing the efficiency and lowering the electricity consumption of cooling systems in CTES can be accomplished through four general approaches:

- Enhancing the insulation of the desired space to reduce heat loss through the use of special insulation panels [4]
- Using a high-efficiency compressor: One of the useful energy management methods is the use of variable speed compressors, which regulate their power consumption based on the cooling load [5].
- Using phase change materials to store cooling energy in the system [6,7]
- Increasing the efficiency of heat exchangers, particularly the evaporator heat exchanger in the refrigeration cycle, which is critical in creating cooling for the CTES technique.

The fourth method, which improves heat exchanger efficiency, appears to be the simplest method for increasing the efficiency of CTES systems and is thus investigated in this study. Heat exchangers are critical components of energy technology, and many studies are focus on improving heat transfer performance in energy technology, such as in References [8–10]. Because of their compact structure and relatively

* Corresponding authors at: Department of Mechanical Engineering, K. N. Toosi University of Technology, Tehran, Iran (S.Seddighi). Linné FLOW Centre, KTH Mechanics, SE-100 44 Stockholm, Sweden (R.Örlü).
*E-mail addresses:* sadeghsk@kth.se (S. Seddighi), orlu@kth.se (R. Örlü).

https://doi.org/10.1016/j.applthermaleng.2021.117559
Received 3 May 2021; Received in revised form 28 July 2021; Accepted 9 September 2021
Available online 20 September 2021
1359-4311/© 2021 The Authors. Published by Elsevier Ltd. This is an open access article under the CC BY license (http://creativecommons.org/licenses/by/4.0/).

**Nomenclature**

| | |
|---|---|
| A | area ($m^2$) |
| Bo | boiling number (-) |
| cp | specific heat capacity (kJ/kg. K) |
| D | diameter (m) |
| d | tube diameter (m) |
| $\dot{E}x_d$ | destructive exergy (W) |
| G | mass flux (kg/$m^2$. s) |
| H | height (m) |
| h | convection heat transfer coefficient (w/$m^2$. K) |
| i | specific enthalpy (J/kg) |
| I | ampere (A) |
| k | thermal conductivity (W/m. K) |
| L | length (m) |
| m | mass (kg) |
| $\dot{m}$ | mass flow rate (kg/s) |
| n | number of coil turns (-) |
| N | number of bubble hole (-) |
| Nu | Nusselt number (-) |
| p | pitch of coil (m) |
| Pr | Prandtl number (-) |
| $\dot{Q}$ | heat transfer rate (W) |
| Re | Reynolds number (-) |
| s | specific entropy (J/kg. K) |
| T | temperature ($^oC$) |
| U | overall heat transfer coefficient (W/$m^2$. K) |
| V | voltage (V) |
| $\dot{V}$ | volumetric flow rate (LPM) |
| W | power consumption (W) |
| $W_R^+$ | uncertainty (-) |
| x | vapor quality (-) |

*Greek symbols*

| | |
|---|---|
| $\Delta T$ | temperature difference ($^oC$) |
| $\mu$ | viscosity (Pa. s) |
| $\rho$ | density (kg/$m^3$) |
| $\varphi$ | angle of bubble injection (rad) |
| $\chi$ | Lockhart–Martinelli parameter |

*Subscripts*

| | |
|---|---|
| b | bubble |
| comp | compressor |
| d | destructive |
| evap | evaporator |
| g | gas |
| i | in |
| if | inner flow |
| l | liquid |
| m | mean |
| o | out |
| of | outer flow (water) |
| ov | overall |
| r | refrigerant |
| sf | evaporator surface |
| st | storage tank |
| w | water |

*Acronyms*

| | |
|---|---|
| COP | coefficient of performance |
| CTES | cold thermal energy storage |
| GWP | Global warming potential |
| LPM | litter per minute |
| NTU | number of thermal units |
| VCRC | Vapor compression refrigeration cycle |

high heat transfer rate, helical coil heat exchangers are widely used in various industries, including food industries, air conditioning, and heat recovery systems [11–13]. Several researchers have worked over the last few decades to improve the performance of Vapor Compression Refrigeration Cycles (VCRC) using a capillary tube [14], nanofluid in the refrigerant and compressor oil [15], and ejector [16]. The VCRC is important in determining cooling demand for residential, industrial, and commercial applications, as well as CTES. Cooling accounts for approximately 10% of global electricity consumption, contributing to 20% of greenhouse gas emissions [17]. Using a helical coil in evaporators is one of the most straightforward methods for improving VCRC performance [18].

Compared to straight coils, the helical coil can increase the heat transfer rate by 60% to 120% [19]. Secondary flow and eddy generation caused by the corrugated walls of the tubes have a significant impact on heat transfer enhancement in the heat exchanger, leading to an increase in overall heat transfer performance of up to 56% [20]. Other factors influencing overall heat transfer performance in helical coil heat exchangers are phase change [21] and local heat transfer distributions inside the coil [22–25]. Although the heat transfer and fluid flow characteristics of the flow inside helically coiled tubes are well covered in the literature, there have been few studies on the thermodynamic and hydrodynamic characteristics of the helical coils' outer surface. Prabhanjan et al. provided an example of such analyses [26]. They investigated heat transfer from a helical coil experimentally and proposed a correlation for the coil's outside Nusselt number based on different characteristic lengths. They reported that the total height of the coil is the best characteristic length that leads to the most accurate correlation. Andrzejczyk et al. [27] used a modular coil heat exchanger in the form of an electric heater to conduct an experimental study on increasing heat transfer in a shell coil heat exchanger with variable baffle geometry. Their experimental results showed that, due to mixed convection, natural convection has a significant effect on small values of Reynolds numbers and large values of Richardson numbers. The location of the buffers was discovered to play an important role in the heat exchanger's performance, and finally, presented new experimental Nusselt number correlations on the shell side of the heat exchanger. Their findings showed that using a baffle geometry increased the efficiency of the shell and helically coiled tube heat exchangers due to secondary flow motion. Tuncer et al. [28] numerically and experimentally investigated a newly modified structure to increase heat transfer from a shell and helically coiled tube heat exchanger. The primary goal of their research [28] was to control the fluid flow on the helical coil and thus increase thermal energy. The results showed that the modified heat exchanger's efficiency was higher than that of the conventional shell and helically coiled tube heat exchangers, with a total heat transfer coefficient in the range of 1600–3150 W/($m^2$. K).

Bubble injection has recently been introduced as a viable solution for improving heat transfer in heat exchangers [29–31]. Bubble injection facilitates the flow transition from laminar to turbulent flow and increases the heat transfer rate [32]. The use of bubble injection can improve the heat transfer rate inside the heat exchanger [29]. The injection mechanism, number of bubbles, geometry, and injection flow rate can all have an impact on the system's heat transfer rate. For the first time, Dizaji et al. [32] used the bubble injection technique to improve heat transfer in a shell and helically coiled tube heat exchanger using water as the working fluid. Spiral geometries with varying numbers of holes were used for bubble injection at a constant flow rate

of 1 LPM. They investigated the effect of bubble injection on the number of thermal units (*NTU*) and the efficiency of the heat exchanger. For bubble injection, four different geometries were used. The results showed that using bubble injection significantly increased the *NTU* and heat exchanger efficiency, which increased up to 1.5–4.2 times in NTU and 1.36–2.44 times in effectiveness compared to pure water (without bubble injection), respectively.

In the study conducted by Dizaji et al. [32], bubble injection was carried out with a constant flow rate of 1 LPM. Therefore, in a similar experiment, Moosavi et al. [33] suggested increasing the injection flow rate to 5 LPM. Their findings indicated that increasing the flow rate of bubble injection had a significant effect on increasing heat transfer. They concluded that increasing the bubble injection flow rate on the shell side could improve the overall heat transfer coefficient by 6%–187% depending on air flow rate. Khorasani and Dadvand [30] devised a novel method for injecting bubbles into a horizontal shell and helically coiled tube heat exchanger. They conducted experiments to determine the effect of bubble injection in the shell side on heat transfer, heat exchanger efficiency, and exergy destruction. In comparison to the case without bubble injection, the results showed that bubbles could increase the *NTU* by up to 4.3 times and the exergy destruction by up to 14.2 times. Injecting bubbles also improved the heat exchanger's efficiency.

Panahi [34] investigated the effect of bubble injection on the Nusselt number and concluded that it could increase heat transfer rate from 50% to 328% compared to the non-bubble injection mode. Pourhedayat et al. [35] investigated the effect of bubble injection on the Nusselt number, exergy destruction, and the efficiency of the heat exchanger with vertical helical coils. Their findings showed that bubble injection increases the Nusselt number, exergy destruction, and heat exchanger efficiency by 57%, 30%, and 45%, respectively. El-said and Alsood [36] investigated the thermal performance and pressure drop of a shell and tube heat exchanger using two cross-flow and co-current air injection techniques. They found that using the cross-flow injection technique increased the overall heat transfer coefficient by 131–171%. It is more efficient than the co-current air injection technique with higher pressure drops. Ökten and Biyikoglu [37] investigated the effect of bubble injection in a water tank on the heat transfer coefficient of the heat exchanger. They discovered that using bubbles doubled the overall heat transfer coefficient between the tank fluid and the coil. In their study, bubbles were injected on both sides of the tube as well as the heat exchanger shell in their experiment. The bubble injection flow rate on the shell side varied from 1 to 5 LPM, while the flow rate on the coil side remained constant at 1 LPM. Heyhat et al. [38] investigated the effect of bubble injection on the performance and exergy analysis of a double pipe heat exchanger. Air bubbles were injected into the annulus side via various injectors. Their findings revealed that using the bubble injection technique significantly improved the efficiency of the heat exchanger, with the overall heat transfer coefficient increasing by up to 149.5%. Ghashim and Flayh [39] experimentally investigated the effect of using bubble injection into the helical coil heat exchanger to examine the heat transfer enhancement and pressure drop. The experiment was carried out in turbulent flow, in a Reynolds number range of 9000–500,000 for hot water and a constant flow rate (0.0331 kg/s) for cold water. Additionally, the bubble volume flow rate ranged between 1.5, 2.5, and 3.5 LPM. They concluded that bubble injection in hot water increased the Nusselt number from 64% to 126% and the pressure dropped from 66% to 85%.

To the best of the authors' knowledge, the thermal performance of the helical coil heat exchanger and the investigation of its heat transfer coefficient under bubble injection in a compression refrigeration cycle or a CTES, as well as the effect of bubble injection on the entire system, have not been investigated. Thus, this study's purpose was to 1) increase the performance of CETS systems by using bubble injection in a helical coil heat exchanger of a VCRC, 2) investigate the effect of using different geometries and flow rates of bubbles on Nusselt number, the amount of heat transferred from the tank, COP of VCRC, and exergy destruction. The VCRC, which is equipped with a helical coil evaporator and is immersed in the water storage tank, serves as the cooling technique in the storage system. A spiral coil with varying flow rates and geometries injects bubbles from the tank's bottom. To reduce the global warming impacts of this system, R1234yf refrigerant was used in the experiments, which had a significantly lower global warming potential (GWP) than R134a.

## 2. Experimental setup and procedure

In this study, a helical coil heat exchanger was used to cool the cold storage water tank. To generate cooling, a compression refrigeration cycle was used. The helical coil heat exchanger is an evaporator that is immersed in a water storage tank and is used to produce cooling. This study's refrigeration cycle experimental setup included a compressor, condenser, expansion valve, and evaporator (storage tank). Fig. 1 depicts a schematic representation of the experimental setup. In this experiment, a direct-current compressor (Secop-BD50F) was used. R1234yf, which is environmentally friendly [40], was used as the refrigerant.

Since the system was small in size, a capillary tube was used instead of an expansion valve. The condenser is a fin tube that is cooled by a fan. This study's test section was the storage tank (evaporator), which was helically coiled and submerged in water. The height and diameter of the water storage tank were both 30 cm ($H_{st} = D_{st} = 30$ cm). The storage tank was also insulated with 15 mm thick polyethylene foam. The outer diameter and the thickness of the copper tubes of the condenser were 6 mm and 0.63 mm, respectively. Table 1 lists the helical coil's characteristics. The bubbles are injected into the storage tank from the bottom of the tank using a spiral coil at various flow rates and geometries (depicted in Figs. 2 and 3). A small air pump (aquarium air pump) with a maximum flow rate and power of 11 LPM and 6.5 W was used to generate the bubbles.

In this test, 5 DS18B20 type sensors with an accuracy of 0.1 °C were used to measure the average temperature of the water in the tank. A polyethylene foam layer insulated the cylindrical storage tank and prevented heat losses to the environment. The storage tank measured 0.28 m in height and diameter. The initial temperature of the water in the storage tank ranged between 22 and 24 °C. The calculated weight of the water was 10.480 kg. Each experiment lasted 2400 s. Furthermore, two similar sensors at the inlet and outlet of the coil were used to measure the evaporator's inlet and outlet temperatures. Since the fluid inside the coil was in a changing phase and the tube was minimal, the inside and outside temperatures of the tube could be considered equal [19]. According to the reports presented in recent works, the pressure drop inside the tubes can be overlooked [41]. Two voltage and ampere sensors with an accuracy of 0.05 A and V were used to measure the compressor's power. A similar sensor was used to activate the fan and regulate the condenser's outlet temperature. Table 2 shows the accuracy and range values of the measurement devices used.

The controlled outlet temperature from the condenser and the condenser's designed temperature were 36 °C and 50 °C, respectively. Figs. 2 and 3 show the schematic diagram of the evaporator helical coil, bubble spiral coil, the geometry and dimensions of the different spiral coils, and evaporator helical coils in experiments. Bubbles were produced by the tiny holes on the helical coils numbered 3, 4, 6, and 8. As shown in Fig. 3, the geometry of the injection can be defined by defining the injection angle (φ) between two rows. For instance, in the case of using eight rows of holes, $\varphi = \pi/4$. The parameter G is defined as the geometry of the bubble injection. The diameter ($D_{air}$) and the thickness of the air tube were 6 mm and 1 mm, respectively. The spiral coil ($D_{spiral}$) and holes diameters ($D_{hole}$) were 250 mm and 1 mm, respectively, and the distance between the rows of the tubes in the spiral coil was 5 mm. A wide range of airflow rates was investigated, ranging from 3 to 11 LPM. A total of 20 different experiments were conducted, and the characteristics of each test are listed in Table 3. An experiment without bubble

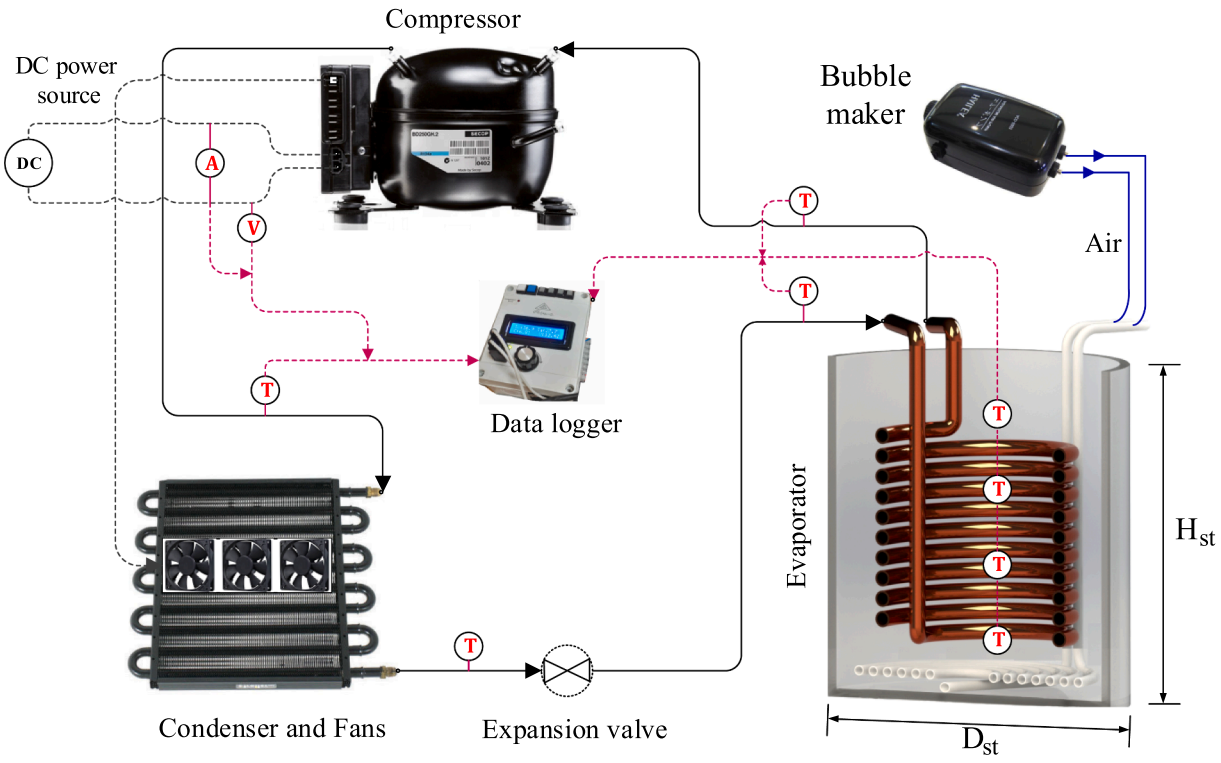


**Fig. 1.** Schematic representation of the experimental setup.

**Table 1**
Characteristics of the helical coil heat exchanger.

| Parameter | Value (mm) |
|---|---|
| Pitch of coil ($p$) | 15 |
| Diameter of coil ($D$) | 142 |
| Tube outer diameter ($d_o$) | 6 |
| Tube inner diameter ($d_i$) | 4.74 |
| Height ($H$) | 168.7 |
| Number of turns ($n$) | 7.75 |

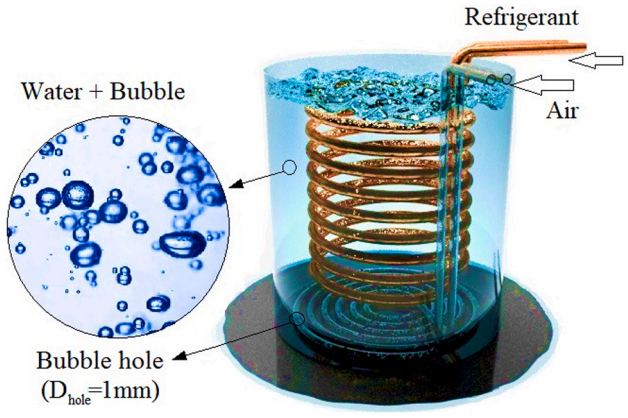


**Fig. 2.** Schematic diagram of the evaporator helical coil and bubble spiral coil in experiments.

injection was carried out to compare the obtained results with those obtained without bubble injection (Test No. 21). It should be noted that the heat transfer rate between the bubbles and the fluid was ignored because the air in bubbles had an insignificant conductivity. In each experiment case, the bubble diameter was determined by the bubble hole diameter and the airflow rate through it, e.g., quantified through $d_b = 358.8\, D_{hole}^{0.296}\, Q^{0.151}$ suggested in Ref. [42]. In this study, the bubble hole diameter was 1 mm, and the airflow rate varied depending on the case. According to the range of air injection flow, the diameter of the bubble was calculated to be between 5.78 and 8.17 mm.

In order to provide further details, different bubble injection geometries (G-3,4,6, and 8) are shown in Fig. 4.

## 3. System analysis and mathematical model

This section describes the method used in this study to process experimental data and calculate various parameters. During the test period, the heat transfer rate from the water in the storage tank to the evaporator coil can be calculated as $\dot{Q}_{evap} = \dot{Q}_{storage} = m_w c_{p,w}\, \Delta T_{of}/\Delta t$, where $m_w$, $c_{p,w}$, and $\Delta T$ are the mass, specific heat capacity, and the temperature difference of the water during the experiment, respectively. The heat transferred to the coil cooled the water in the storage tank. On the other hand, the absorbed heat by the coil can be obtained using $\dot{Q}_{evap} = \dot{m}_r(i_{if,out} - i_{if,in})$, where $\dot{m}_r$ and i are the refrigerant mass flow rate and the specific enthalpy, respectively.

Therefore, the refrigerant mass flow rate can be calculated by determining the thermodynamic state of the fluid at the coil's inlet and outlet. The injection of bubbles was expected to increase the heat transfer coefficient due to the transition from laminar to turbulent flow [32]. It should be noted that the heat transfer calculations of air bubbles to water in the storage tank were overlooked due to the low heat capacity of air against water [31,43]. To calculate the outside heat transfer coefficient of the coil, the overall heat transfer coefficient ($U_{ov}$) should be introduced, i.e.,

$$U_{ov} = \dot{Q}_{evap}/(A_o \Delta T_m) \quad (1)$$

where $\Delta T_m$ and $A_o$ are the mean temperature difference and the outside area of the coil, respectively, and can be calculated as follows [44]:

$$A_o = n\pi d_o \sqrt{p^2 + \pi^2 D^2} \quad (2)$$

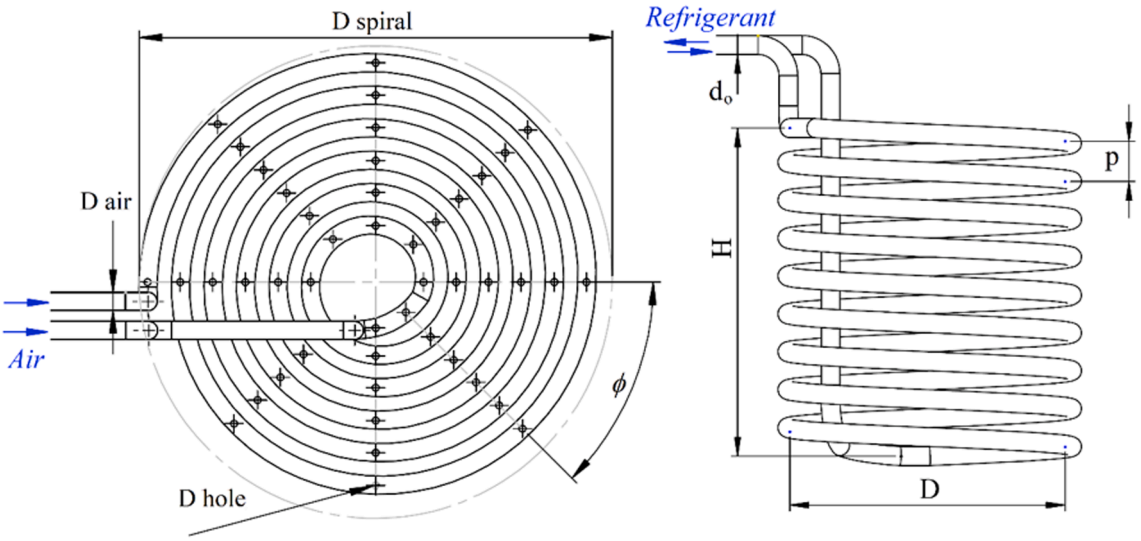


**Fig. 3.** Geometry and dimensions of the different spiral coils and evaporator helical coils in experiments.

**Table 2**
Accuracy and range values of utilized measurement devices.

| Measurement device | Range value | Accuracy |
|---|---|---|
| Temperature | [−55 to 125] °C | 0.1 °C |
| Voltage | [2 –30] V | 0.05 V |
| Current | [0–30] A | 0.05 A |
| Length | [0–0.5] m | 0.0001 m |
| Mass (of water) | [0–2] kg | 0.02 kg |

**Table 3**
Characteristics of each test experiment (geometry of coil and air bubble injection conditions).

| Test No. | Geometry | φ (rad) | Airflow rate (LPM) | $N_{hole}$ |
|---|---|---|---|---|
| 1 | G-6 | $\pi/3$ | 3 | 36 |
| 2 | G-6 | $\pi/3$ | 5 | 36 |
| 3 | G-6 | $\pi/3$ | 7 | 36 |
| 4 | G-6 | $\pi/3$ | 9 | 36 |
| 5 | G-6 | $\pi/3$ | 11 | 36 |
| 6 | G-3 | $2\pi/3$ | 3 | 18 |
| 7 | G-3 | $2\pi/3$ | 5 | 18 |
| 8 | G-3 | $2\pi/3$ | 7 | 18 |
| 9 | G-3 | $2\pi/3$ | 9 | 18 |
| 10 | G-3 | $2\pi/3$ | 11 | 18 |
| 11 | G-8 | $\pi/4$ | 3 | 48 |
| 12 | G-8 | $\pi/4$ | 5 | 48 |
| 13 | G-8 | $\pi/4$ | 7 | 48 |
| 14 | G-8 | $\pi/4$ | 9 | 48 |
| 15 | G-8 | $\pi/4$ | 11 | 48 |
| 16 | G-4 | $\pi/2$ | 3 | 24 |
| 17 | G-4 | $\pi/2$ | 5 | 24 |
| 18 | G-4 | $\pi/2$ | 7 | 24 |
| 19 | G-4 | $\pi/2$ | 9 | 24 |
| 20 | G-4 | $\pi/2$ | 11 | 24 |
| 21 | – | – | 0 (non-bubble) | – |

$$\Delta T_m = T_{of} - 0.5 \times (T_{if,in} + T_{if,out}) \tag{3}$$

where $T_{of}$, $T_{if,in}$ and $T_{if,out}$ are the water temperature in storage tank, evaporator inlet and outlet temperature, respectively. Therefore, by calculating the overall heat transfer coefficient and the thermal resistance from the refrigerant to the water, the heat transfer coefficient outside the coil can be obtained [45]:

$$h_{of} = \left[\frac{1}{U_{ov}} - \frac{d_o}{d_i\, h_r} - \frac{d_o ln\,(d_o/d_i)}{2k_{tube}}\right]^{-1} \tag{4}$$

In this equation, $h_r$, $h_{of}$, and $k_{tube}$ are the heat transfer coefficients of the refrigerant, water, and conductivity of the copper tube, respectively. Furthermore, because the thermal resistance and thickness of the tube were too small, the outside and inside temperatures of the tube can be considered equal. [19]. The Nusselt number of fluid during the phase transition can be calculated as follows [46]:

$$h_r/h_l = 2.84\chi_{tt}^{-0.27} + (4616Bo - 0.88) \tag{5}$$

where $Bo$, $h_l$ and $\chi_{tt}$ are the boiling number, heat transfer coefficient inside the coil (in single-phase state), and Lockhart-Martinelli parameter, respectively, and can be defined as follows:

$$h_l = 0.023Re^{0.85}Pr^{0.4}(d_o/D)^{0.1} \tag{6}$$

$$\chi_{tt} = \left(\frac{1-x}{x}\right)^{0.9}\left(\frac{\rho_g}{\rho_l}\right)^{0.5}\left(\frac{\mu_l}{\mu_g}\right)^{0.1} \tag{7}$$

$$Bo = \frac{\dot{Q}_{evap}}{A_o G(i_g - i_l)} \tag{8}$$

where Re, Pr, x, ρ and μ are the Reynolds number, Prandtl number, vapor quality, density and viscosity of refrigerant. In these equations, G is the mass flux and is defined as:$G = \dot{m}_r/A_{if}$ where $A_{if}$ is the inner tube area of the evaporator helical coil. Therefore, the heat transfer rate from the outside of the coil can be calculated using the heat transfer coefficient inside the coil (using Eq. (4)).

The absorbed heat by the evaporator had a direct relationship with the heat transfer rate from the outside of the coil. Therefore, the Nusselt number of the outside of the coil ($Nu_{of}$) was used to compare the various cases of the experiment. The Nusselt number was defined according to the following equation:

$$Nu_{of} = \frac{h_{of}L}{k_{of}} \tag{9}$$

Since the helical coil is the evaporator of the refrigeration cycle, the *COP* can be a suitable parameter for comparing the performance of the refrigeration cycle in various experiments, which can be defined as follows:

$$COP = \frac{\dot{Q}_{evap}}{W_{comp} + W_{bubble}} \tag{10}$$

where $W_{comp}$ and $W_{bubble}$ are the power consumed by the fanned

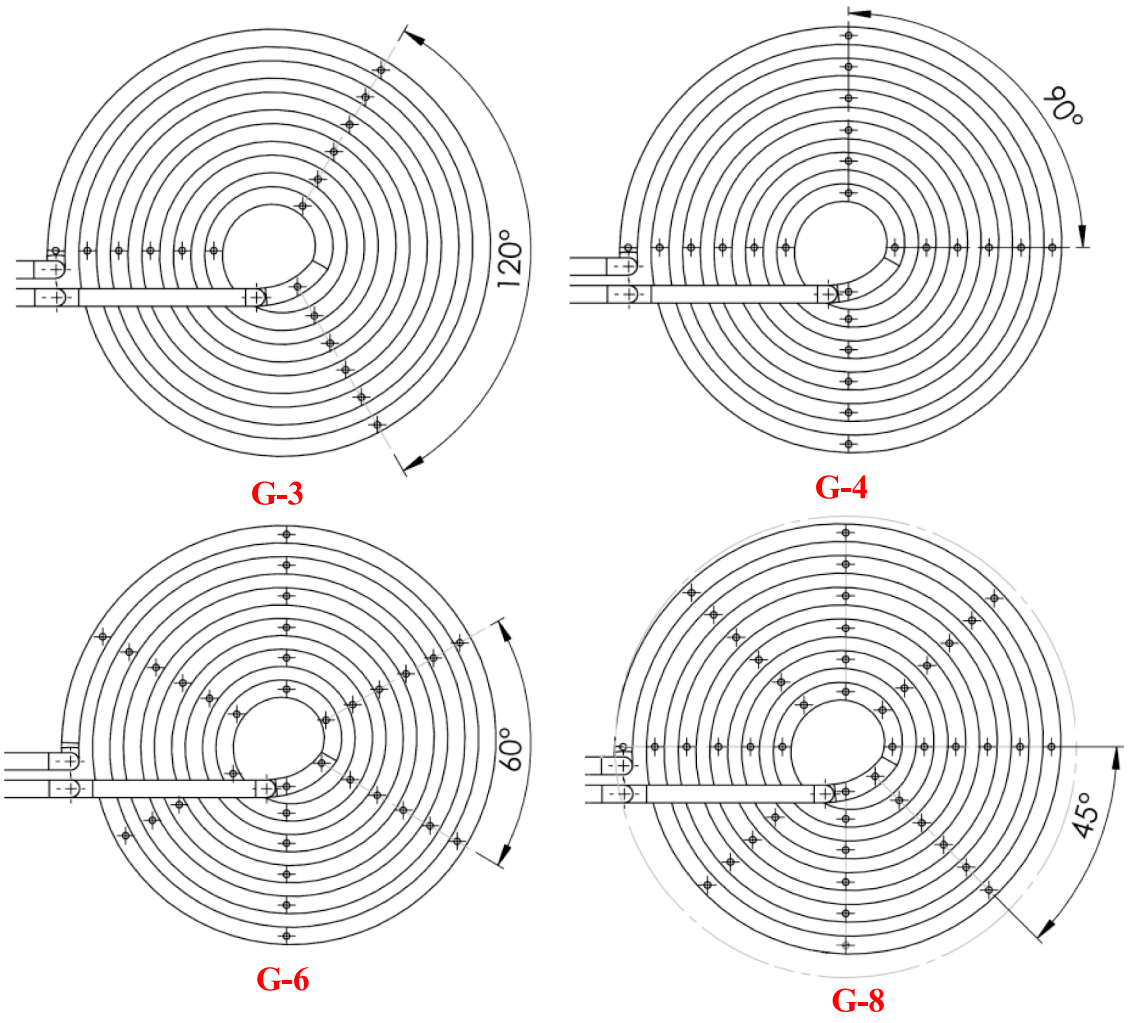


**Fig. 4.** Different bubble injection geometries.

compressor and the bubble generator pump, respectively. The fans are powered by the auxiliary ports on the controller board of the compressor. Therefore, the power consumption of the compressor and the fans are measured together. In this experiment, the amount of heat absorbed by the evaporator was changed by varying the flow rate of the bubble generator. The exergy destruction rate($\dot{E}x_d$)can also be calculated as follows [47]:

$$\dot{E}x_d = \dot{m}_r[(i_{if,out} - i_{if,in}) - T_0(s_{if,out} - s_{if,in})] + \dot{Q}_{evap}(1 - T_0/T_{sf}) \quad (11)$$

where s and $T_{sf}$ are the specific entropy and the evaporator temperature, respectively. Errors can occur in any experimental measurement due to measurement equipment uncertainties and operator error. Thus, calculating the uncertainty of the variables is critical. The degree of uncertainty indicates how far the obtained results differ from their actual values. In the present study, the uncertainty of the parameters was evaluated according to Eq. (12) [48], and the results are listed in Table 4.

$$W_R^+ = \left[\sum_{i=1}^{n}\left(\frac{\partial R}{\partial x_i}W_i\right)^2\right]^{0.5} \quad (12)$$

where $W_R^+$ and $W_i$are the uncertainty of variable R and $x_i$, respectively.

**Table 4**
Uncertainty in variables.

| Parameters | | Uncertainly |
|---|---|---|
| Measured variable | Ampere ($I$) | 0.05 A |
| | Voltage ($V$) | 0.05 V |
| | Temperature ($T$) | 0.1 °C |
| | Mass ($m_w$) | 0.02 kg |
| | Length ($L$) | 0.0001 $m$ |
| Calculated variable | $COP$ | 3.70% |
| | $\dot{Q}_{evap}$ | 3.68% |
| | $\dot{E}x_d$ | 3.80% |
| | $Nu_{of}$ | 4.64% |

## 4. Result and discussion

### 4.1. The effect of bubble injection

Fig. 5 shows the effect of air bubble flow rate on the outside Nusselt number of the coil ($Nu_{of}$) for various bubble injection geometries. Based on the figure, it can be concluded that:

- The generated small-sized bubbles had three effects on the heat transfer from the coil: 1) the generated bubbles moved upward due to the buoyancy force, resulting in a homogeneous temperature distribution inside the tank, and had a positive effect [33,34]. 2) the bubbles acted as turbulators and, consequently, enhanced the heat

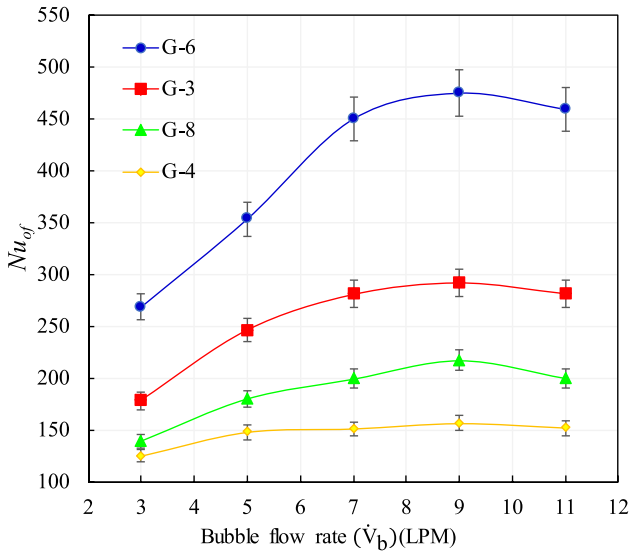


**Fig. 5.** The effect of $\dot{V}_b$on the $Nu_{of}$ for different bubble injection geometries.

transfer rate from the coils [49]. 3) The amount of bubble was so great at high injection flow rates that it isolated the coil and separated it from the surrounding water, impeding heat transfer. Therefore, for maximum heat transfer, an optimum bubble injection rate was to be used.

- The optimal bubble injection flow rate for maximum heat transfer was 9 LPM. The $Nu_{of}$ was improved by increasing the bubble injection rate from 3 to 9 LPM.
- It can be seen that the slope of the variations of Nusselt number in lower injection flow rates is relatively higher in lower injection flow rates than in higher flow rates due to the dynamic of the bubble movement and the effect of the turbulence on the thermal boundary layer around the coil. If the bubble is not injected into the water tank, natural convection dominates the heat transfer mechanism, with a lower Nusselt number than the mixed and forced convection mechanisms [24,49]. When bubbles are injected at low flow rates, the flow mechanism is mixed convection, and there is still a natural convection effect. The flow regime shifts from mixed and natural convection to forced convection as the airflow rate increases. As previously stated, the Nusselt number rises dramatically as a result of the transition to a turbulent regime. The Nusselt number decreases as the flow rate of bubble injection increases, isolating the coil from water by bubbles. Therefore, changes in the Nusselt number during the initial phase of the injection are more noticeable. Ref. [50] provides further information on the dynamics of bubbles.

Fig. 6 compares the Nusselt number in various bubble injection geometries and the non-bubble injection mode at a flow rate of 9 LPM. It can be concluded that increasing the number of holes does not always increase the heat transfer rate and system performance. Reducing the number of holes can help to increase the speed of the bubbles and the rate of heat transfer. Reducing the number of holes and increasing the speed of the bubbles, on the other hand, results in the isolation of the helical coil from the water and, as a result, a decrease in system performance. Therefore, in order to achieve the best possible condition, a trade-off between these two effects must be made. The optimum geometry and injection flow rate in this study was G-6, with a flow rate of 9 LPM. Obviously, by increasing the $Nu_{of}$ compared to the non-injection mode, it reached 4.5 times in G-6 geometry.

Fig. 7 shows the relationship between $Nu_{of}$ and *COP* of the cycles. As the heat transfer coefficient increases, so does the amount of heat taken; thus, increasing the $Nu_{of}$ has a direct relationship with increasing the COP. Increasing the $Nu_{of}$ improves the COP by increasing the heat

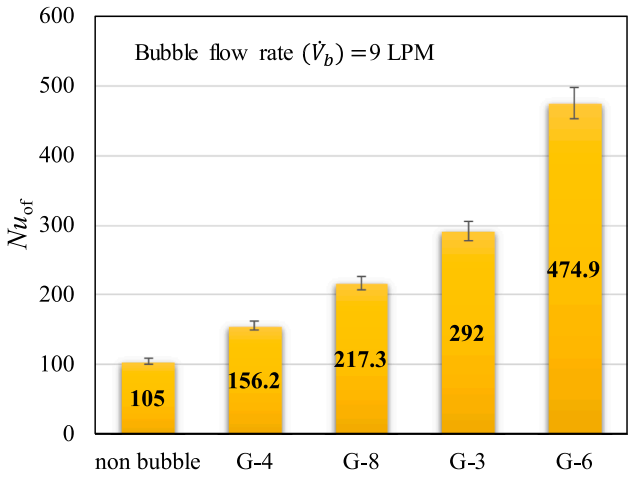


**Fig. 6.** The effect of air bubble injection geometry on the $Nu_{of}$ at $\dot{V}_b$ = 9LPM.

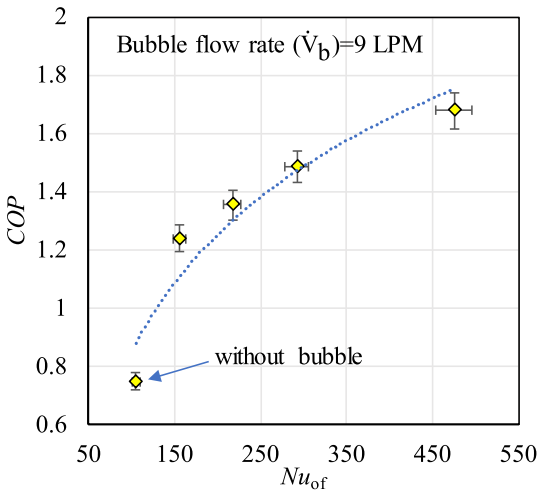


**Fig. 7.** Variation of *COP* as a function of $Nu_{of}$ at $\dot{V}_b$ = 9 LPM.

transfer rate in the evaporator. Using bubble injection improves the *COP* of the cycle, which improves the cooling capacity of the system and lowers the costs. This increase in *COP* and $Nu_{of}$ is determined by the geometry and the rate of bubble injection. In comparison to the non-bubble injection mode, the COP of the cycle increased from 65% to 123% at 9 LPM injection flow rate and different injection geometries.

Table 5 shows the *COP* results of the cycle as a result of bubble injection in various flows and geometries. Since the increase in $Nu_{of}$ and *COP* are co-directional, the highest *COP* occurred in the highest $Nu_{of}$. The percentage increase in *COP* is shown in the table when compared to the non-bubble injection mode (as an average in each geometry). The heat transfer rate from the water to the evaporator increases as the Nusselt number increases. Thus, increasing the Nusselt number results in

**Table 5**
Result of COP at different bubble flow rate and geometry.

| Bubble flow rate ($\dot{V}_b$) (LPM) | COP | | | |
|---|---|---|---|---|
| | G-6 | G-3 | G-8 | G-4 |
| 3 | 1.3 | 1.13 | 1.07 | 1.05 |
| 5 | 1.38 | 1.31 | 1.23 | 1.15 |
| 7 | 1.61 | 1.38 | 1.26 | 1.2 |
| 9 | 1.68 | 1.49 | 1.35 | 1.24 |
| 11 | 1.59 | 1.41 | 1.25 | 1.15 |
| Without bubble | 0.75 | | | |
| % Increase (average) | **101.5** | **78.7** | **64.14** | 54.5 |

an increase in the *COP*.

Fig. 8 indicates the variation of the water storage tank compared to the initial water temperature ($\Delta T_{of}$) during the experiment. According to the previous explanations, the system with the geometry of G-6 has the highest Nusselt number and *COP*. Therefore, the temperature difference of this case (5.05 ℃) is relatively higher than in other cases. As can be seen, the geometry of the bubbles plays an important role in increasing the heat transfer rate.

Fig. 9 depicts the effect of different flow rates and bubble injection geometry on storage water temperature differences. As expected, increasing the Nusselt number increases the amount of heat extracted from the water. The G-6 geometry had the greatest temperature difference at all injection flow rates, as shown in the figure. Furthermore, the maximum temperature increase at the end of the experiment time (t = 2400 s) compared to the non-bubble injection mode was 2.3°, and the minimum was 0.98°, increasing by 83.6% and 35.6%, respectively.

Fig. 10 shows the evaporator destructive exergy ratio (compared to the non-bubble injection mode) as a function of bubble flow rate at various bubble injection geometries. According to the definition of entropy, increasing the flow rate results in an increase in destructive exergy. On the other hand, the heat transfer rate and evaporator capacity both increased. Therefore, the overall impact of bubble injection is positive. The destructive exergy is affected by several parameters, including the geometry and the flow rate of the bubble injection. According to Fig. 10, G-6 has the highest amount of exergy destruction, owing to the dynamic of the bubbles and their movement speed, because moving bubbles around the coil at different velocities and bubble volumes can cause degraded exergy destruction changes. As shown, the destructive exergy ratio increased up to 2.25 times when compared to the no bubble injection mode. Furthermore, if the airflow rate remains constant, increasing the number of holes reduces the speed of the bubbles and, as a result, the heat transfer.

Fig. 11 depicts the heat rate obtained from CTES in various geometries and at the optimum injection flow rate (9 LPM). This figure illustrates the effect of bubble injection on increasing the rate of stored cold. The cold storage rate was 50.3 W without bubble injection and 92.4 W with bubble injection, a 96.9% increase depicts the effect of bubble injection flow on the percentage increase in the rate of cold stored in the storage tank for various geometries in comparison to the non-bubble injection mode. As it turns out, the rate of increase is determined by the bubble injection mechanism. G-6 geometry increased the most significantly, while G-4 geometry increased the least. Therefore, bubbles can increase the temperature stored in CTES by at least 23.1% and up to 96.9%, resulting in lower operating costs (see Fig. 12).

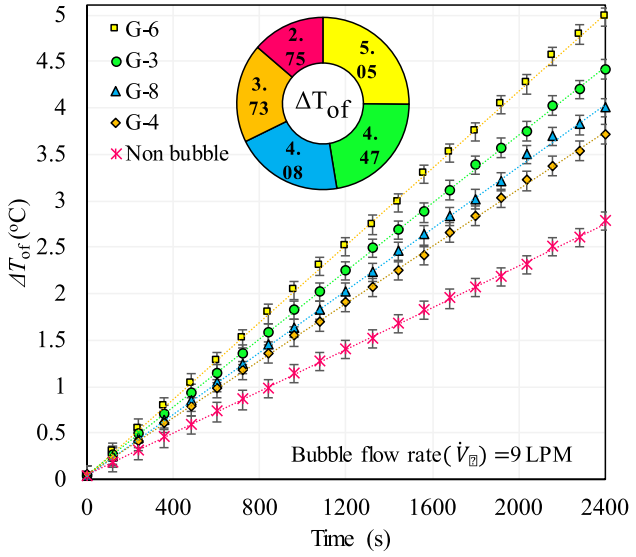


**Fig. 8.** The variation of the water storage tank compared to the initial water temperature ($\Delta T_{of}$) during the experiment at $\dot{V}_b$ = 9 LPM. Numbers in the annular pie chart indicate the respective value after 2400 seconds.

The variation of evaporator temperature ($T_{sf}$), condenser outlet temperature ($T_{sub}$), and compressor power consumption ($W_{comp}$) during the test time for experiment No. 4 are depicted in Fig. 13, Fig. 14, and Fig. 15, respectively. After a while, the evaporator temperature stabilized and remained constant until the test ended. Therefore, the evaporator analysis in steady-state mode is correct. In addition, the outlet temperature from the condenser had an average value with oscillations due to the cooling with the fan, which turned on and then off as the temperature rose above the design limit. Temperature oscillations were small, as shown in the figure, and did not affect the refrigeration cycle or compressor operation.

In all of the studied compression refrigeration cycles, the compressor operated until the evaporator ambient temperature reached a certain value (specified by the thermostat), at which point it turned off and then on. As a result of this research's application, the temperature of the evaporator storage tank could always be kept at the desired temperature by using a thermostat. Consequently, the system was able to operate for a long time.

### 4.2. Nusselt number correlation

This section presents a new correlation for the coil's outside Nusselt number based on experimental data. The following correlation was proposed in this study for Nusselt number ($Nu_{of}$) as a function of flow rate and geometry of the injected bubbles:

$$Nu_{of} = a \times exp\left[-\left(\frac{(Re_b - b)}{c}\right)^2\right]$$
$$Re_b = 4(\dot{V}_b/N_{hole})/(\mu_{air}\pi D_{hole}) \quad (13)$$
$$3 \leqslant \dot{V}_b(LPM) \leqslant 11$$

where a, b, and c are fixed coefficients that depend on the bubble injection angle ($\varphi$), and the values of these parameters are given in Table 6. Additionally, in Eq. (13), $N_{hole}$, $\mu_{air}$, $D_{hole}$ are the number of bubble holes, air viscosity, and the diameter of the bubble injection hole, respectively.

According to Table 6, changes in bubble injection angle ($\varphi$) play a vital role in Nusselt number ($Nu_{of}$) changes. Fig. 16 shows the comparison of the experimental Nusselt number with the predictions of the proposed correlation. According to this figure, the proposed equation's highest error is 5.8%, which is an acceptable amount for experimental correlation. Furthermore, as previously stated, the changes in COP with $Nu_{of}$ are in the same direction. The results show a power-law correlation between *COP* and $Nu_{of}$ number (Eq. (14)). Therefore, by calculating the $Nu_{of}$, the *COP* can be calculated. Given that the $Nu_{of}$ is a function of φ and bubble flow rate, the calculated *COP* is also a function of those parameters.

$$COP = 0.2076\, Nu_{of}^{0.3245} + 0.09141$$
$$R^2 = 0.92 \quad (14)$$

Table 7 compares the present study's findings to those of other studies published in the literature. The maximum increase in Nusselt number as a result of bubble injection in the heat exchanger was taken into account. As shown in the table, using the present method, the Nusselt number can be increased by up to 452% (compared to the non-bubble injection mode).

## 5. Conclusion

This work experimentally studied the heat transfer augmentation using bubble injection in cold thermal energy storage system application using a helical coil heat exchanger. An immersed helical coil heat

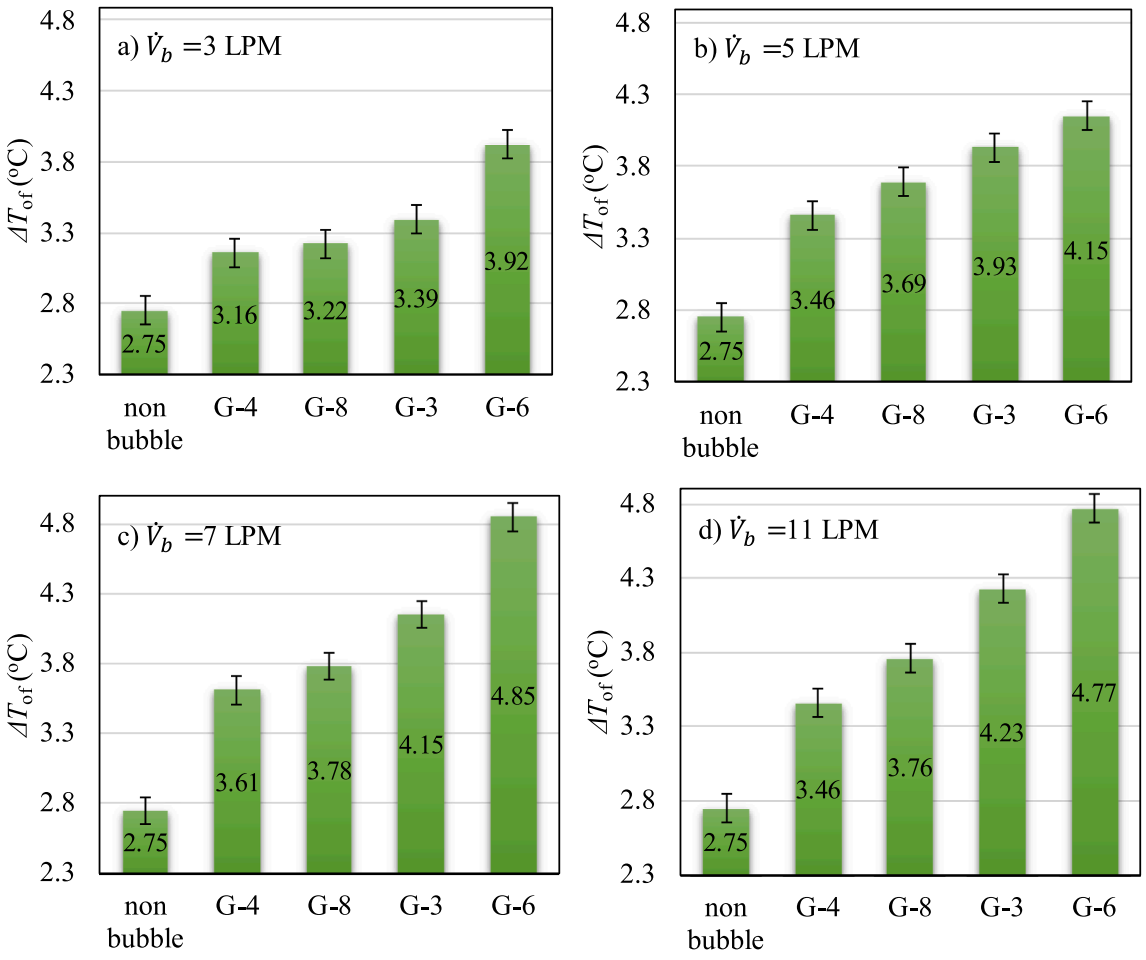


**Fig. 9.** The effect of bubble injection geometry on the storage tank temperature difference ($\Delta T_{of}$) at different Bubble flow rate ($\dot{V}_b$).

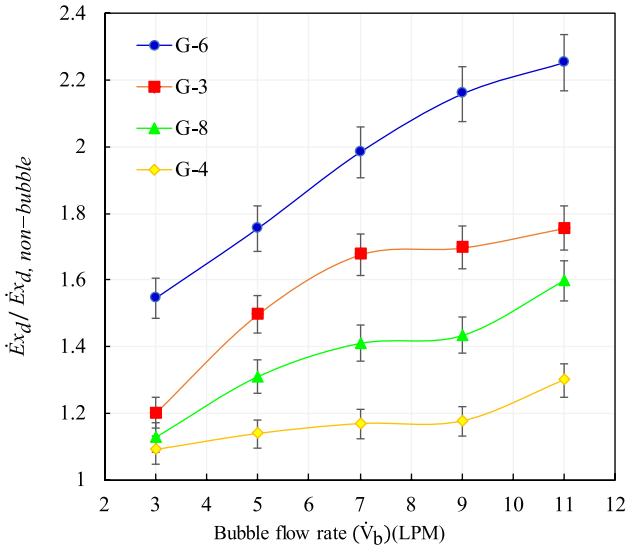


**Fig. 10.** Normalized evaporator destructive exergy ratio as a function of $\dot{V}_b$ at different bubble injection geometries.

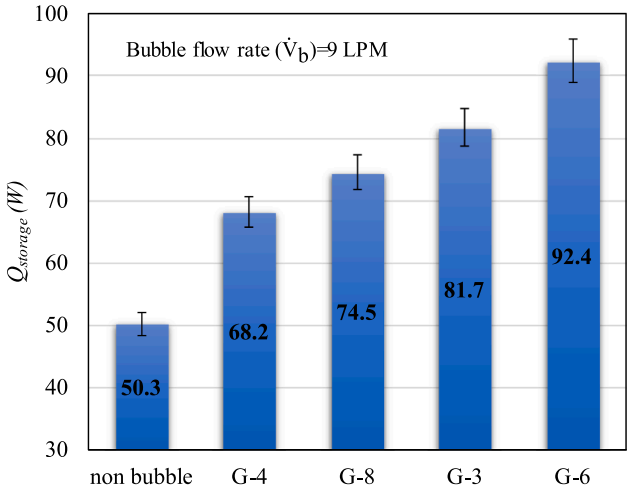


**Fig. 11.** The effect of bubble injection geometry on the $Q_{storage}$ at $\dot{V}_b$ = 9 LPM and $\dot{V}_b$ = 0 LPM (without bubble injection).

exchanger in a water storage tank was used for cooling, which was the evaporator of the compression refrigeration cycle. The bubbles were injected into the storage tank using an air pump through a spiral coil. Four different geometries and a wide range of mass flow rates ranging between 3 and 11 LPM for bubble injection were investigated. The compression refrigeration cycle's evaporator was cooled using an immersed helical coil heat exchanger in a water storage tank. Using an air pump and a spiral coil, the bubbles were injected into the storage tank. For bubble injection, four different geometries and a wide range of flow rates ranging from 3 to 11 LPM were investigated. The experiments were carried out to determine the effect of bubble injection on the rate of heat taken, the outside Nusselt number of the coil ($Nu_{of}$), the *COP* of the

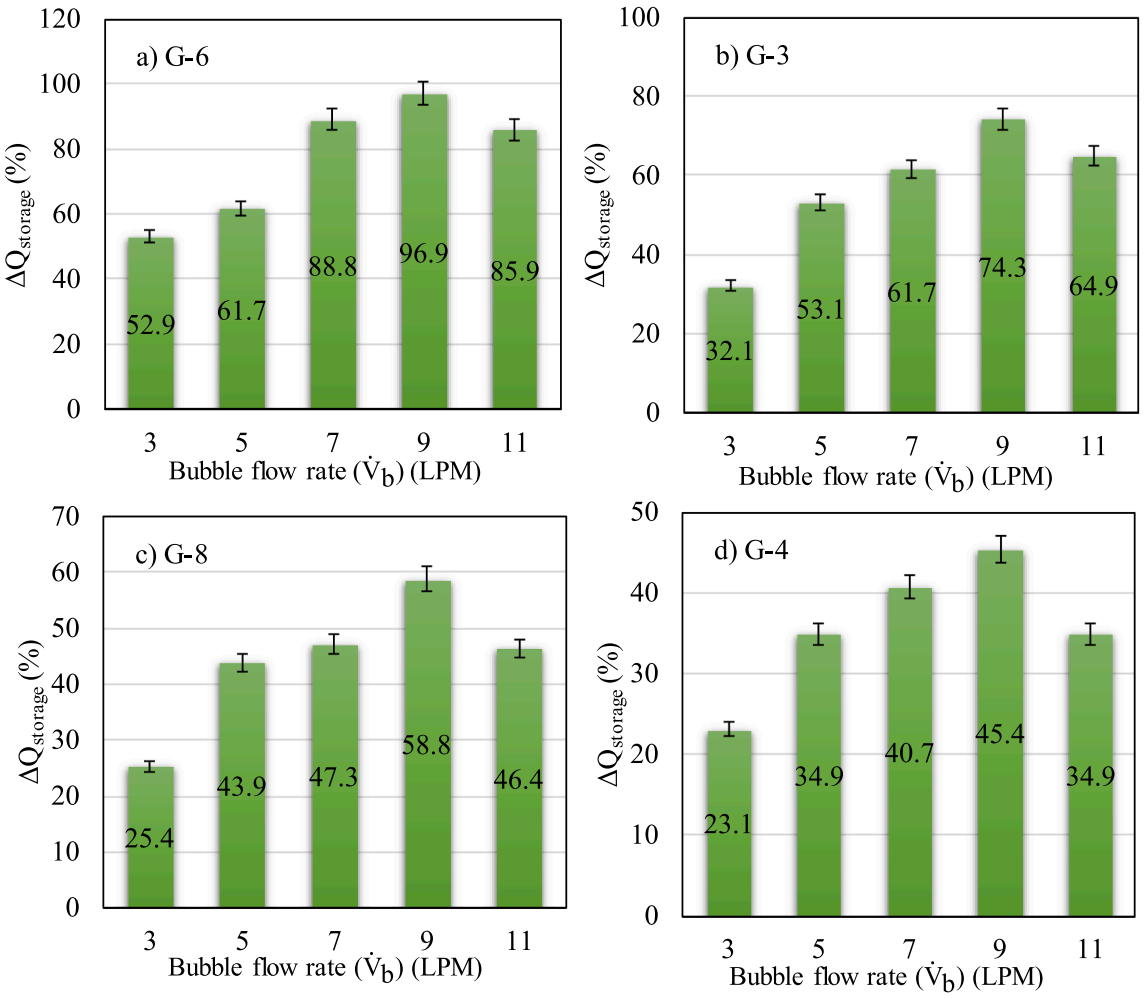


**Fig. 12.** The effect of $\dot{V}_b$ on the percentage of $Q_{storage}$ increase ($\Delta Q_{storage}$), at different injection geometries.

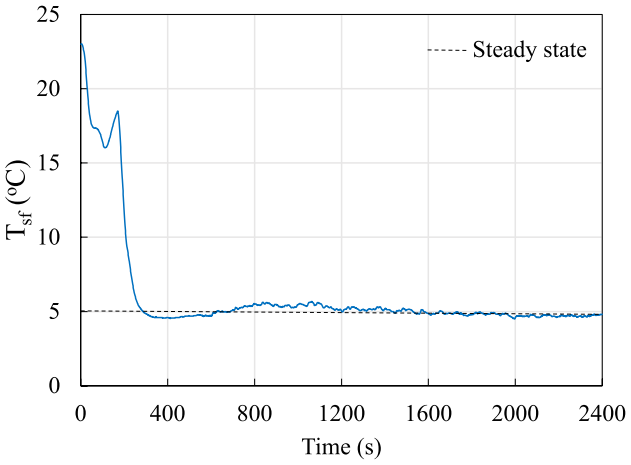


**Fig. 13.** Variation of evaporator temperature ($T_{sf}$) during the test time.

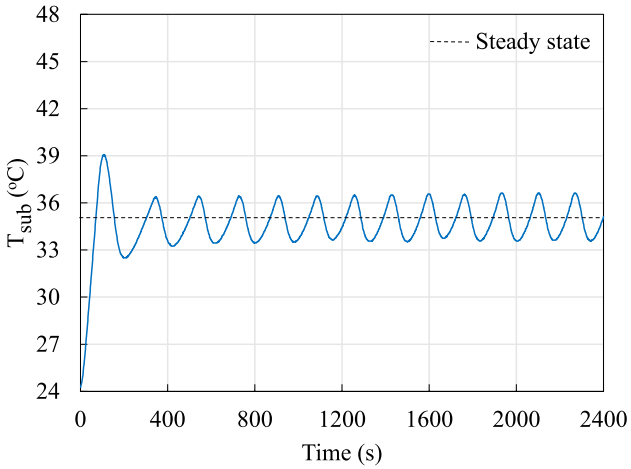


**Fig. 14.** Variation of condenser outlet temperature ($T_{sub}$) during the test time.

cycle, and the destructive exergy in the storage tank. This study's findings can be summarized as follows:

- The use of bubble injection had a significant impact on the coil's outside Nusselt number ($Nu_{of}$). This increase was heavily influenced by the geometry and flow rate of the injected bubbles. Compared to the non-bubble injection mode, using the bubble increased the $Nu_{of}$ by up to 4.52 times. The findings also revealed that the changes in COP with $Nu_{of}$ were pointing in the same direction. The COP rate increased from 40 to 101.5% when the bubble injection flow rate was increased from 3 to 11 (LPM).
- The Nusselt number increased when the airflow rate was increased from 3 LPM to 9 LPM. However, further increase in the bubble air flowrate from 9 to 11 LMP resulted in decreased heat transfer

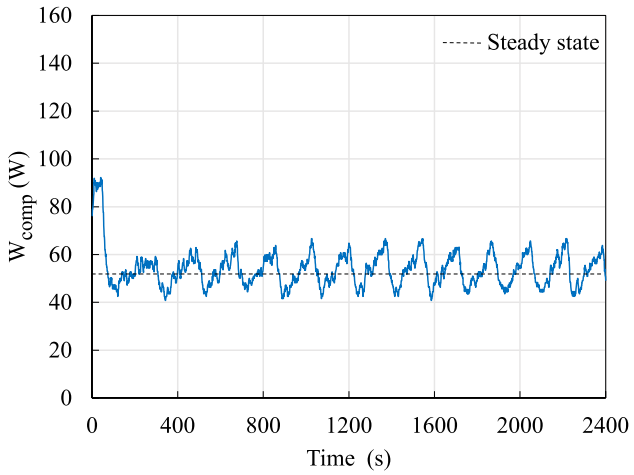


**Fig. 15.** Variation of compressor power ($W_{comp}$) during the test time.

**Table 6**
The result of constant coefficients (a,b, and c) in Eq.(13).

| $\varphi$ | geometry | a | b | c | $R^2$ | max $Nu_{of}$ |
|---|---|---|---|---|---|---|
| $\pi/3$ | G-6 | 478.6 | 348.3 | 306.8 | 0.99 | 474.9 |
| $2\pi/3$ | G-3 | 296.4 | 666.4 | 634.6 | 0.99 | 292 |
| $\pi/4$ | G-8 | 213.2 | 248.1 | 251.4 | 0.98 | 217.3 |
| $\pi/2$ | G-4 | 156.7 | 486.7 | 693.7 | 0.95 | 156.2 |

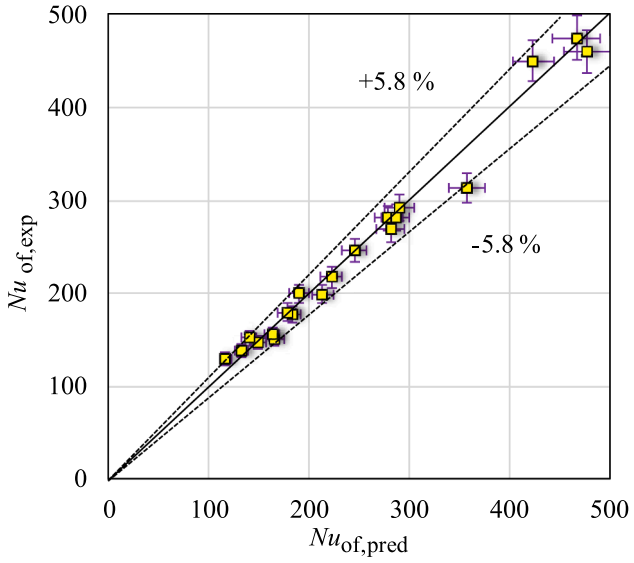


**Fig. 16.** The comparison of the experimental Nusselt number with the predictions of the proposed correlation (Eq. (13)).

coefficient due to the isolation of the coil with bubbles. Moreover, at a 9 LPM injection flow rate and in different injection geometries, the *COP* cycle increased from 65% to 124% compared to the non-bubble injection mode.

- The results showed that in all cases, the use of bubbles increased the destructive exergy in the evaporator so that it increased up to 2.25 times compared to the non-bubble injection case.
- The findings revealed that increasing the number of bubble holes does not always result in increased heat transfer. It was also discovered that at lower bubble flow rates, the slope of the Nusselt number change is steeper.

**Table 7**
The comparison of the increase in *Nu* number obtained in the present study with other investigations.

| Research | Experiment description | Increase in *Nu* |
|---|---|---|
| Dizaji et al. [51] | Effects of air bubble injection on heat transfer in a horizontal double pipe heat exchanger were investigated. Bubble injection was carried out in both inner (hot fluid) and outer tubes (cold fluid). They concluded that the best results are obtained when air bubbles are injected into the annular space between two tubes (outer tube). | 35% |
| Pourhedayat et al.[35] | Performance of a vertical double-tube heat exchanger with bubble injection was investigated. Bubbles of varying diameters were injected at a constant flow rate into the annular space between two vertical tubes (outer tube) connected by a circular ring at the heat exchanger's bottom. Maximum effectiveness was obtained as the number of holes in the circular ring increased and the diameter of the holes decreased. | 57% |
| Ghashim et al. [39] | Experimental investigation of heat transfer enhancement in a heat exchanger due to the injection of air bubbles was studied. A counter-current double coiled (multi-coil) heat exchanger was used, and the bubbles were injected with different flow rates into the hot fluid tube. Injecting air bubbles into the heat exchanger was found to improve its efficiency. | 126% |
| Panahi [34] | Nu number of a vertical shell and coiled tube heat exchanger was increased using air bubble injection. To inject the bubbles, they used a helical coil heat exchanger surrounded by water inside the shell and a spiral coil placed at the bottom of the shell. Bubble injection improved the heat exchanger's effectiveness and Nusselt number. The amount of these increases was determined by the air injection condition and the shell side Reynolds number. | 328% |
| **Present study** | To increase Nu number, air bubbles were injected over a vertical helical coiled tube in a water tank. The helical coil is the evaporator of a vapor compression refrigeration cycle (VCRC) and provides the designed cooling in the cold thermal energy storage (CTES) system. | **452%** |

- The use of bubbles was shown to increase the rate of stored cold by at least 23.1% and up to 96.89% compared to the non-bubble injection mode.

## Declaration of Competing Interest

The authors declare that they have no known competing financial interests or personal relationships that could have appeared to influence the work reported in this paper.

## References

[1] S.-F. Li, Z.-H. Liu, X.-J. Wang, A comprehensive review on positive cold energy storage technologies and applications in air conditioning with phase change materials, Appl. Energy 255 (2019), 113667.
[2] O.G. Zarajabad, R. Ahmadi, Numerical investigation of different PCM volume on cold thermal energy storage system, J. Storage Mater. 17 (2018) 515–524.
[3] M. MacCracken, Energy storage: providing for a low-carbon future, ASHRAE J. 52 (9) (2010) 28–34.
[4] S. Verma, H. Singh, Vacuum insulation panels for refrigerators, Int. J. Refrig 112 (2020) 215–228.
[5] P. Su, J. Ji, J. Cai, Y. Gao, K. Han, Dynamic simulation and experimental study of a variable speed photovoltaic DC refrigerator, Renew. Energy 152 (2020) 155–164.
[6] A. Aljehani, S.A.K. Razack, L. Nitsche, S. Al-Hallaj, Design and optimization of a hybrid air conditioning system with thermal energy storage using phase change composite, Energy Convers. Manage. 169 (2018) 404–418.
[7] X. Wan, C. Chen, S. Tian, B. Guo, Thermal characterization of net-like and form-stable ML/SiO2 composite as novel PCM for cold energy storage, J. Storage Mater. 28 (2020), 101276.

[8] D. Maggiolo, S. Sasic, H. Ström, Self-cleaning compact heat exchangers: the role of two-phase flow patterns in design and optimization, Int. J. Multiph. Flow 112 (2019) 1–12.
[9] A. Coppola, F. Scala, A Preliminary Techno-Economic Analysis on the Calcium Looping Process with Simultaneous Capture of CO2 and SO2 from a Coal-Based Combustion Power Plant, Energies 13 (9) (2020) 2176.
[10] F. Mallor, M. Raiola, C.S. Vila, R. Örlü, S. Discetti, A. Ianiro, Modal decomposition of flow fields and convective heat transfer maps: An application to wall-proximity square ribs, Exp. Therm Fluid Sci. 102 (2019) 517–527.
[11] X. Liu, X. Xu, C. Liu, W. Bai, C. Dang, Heat transfer deterioration in helically coiled heat exchangers in trans-critical CO2 Rankine cycles, Energy 147 (2018) 1–14.
[12] K. Ökten, B. Kurşun, A. Toksöz, M. Kara, Analysis of coiled tube waste heat storage tank under water injection, J. Storage Mater. 26 (2019), 100979.
[13] A. Fouda, S. Nada, H. Elattar, H. Refaey, A.S. Bin-Mahfouz, Thermal performance modeling of turbulent flow in multi tube in tube helically coiled heat exchangers, Int. J. Mech. Sci. 135 (2018) 621–638.
[14] L. Lorbek, A. Kuhelj, M. Dular, A. Kitanovski, Two-phase flow patterns in adiabatic refrigerant flow through capillary tubes, Int. J. Refrig 115 (2020) 107–116.
[15] V. Nair, A. Parekh, P. Tailor, Experimental investigation of a vapour compression refrigeration system using R134a/Nano-oil mixture, Int. J. Refrig 112 (2020) 21–36.
[16] Q. Chen, Y. Hwang, G. Yan, J. Yu, Theoretical investigation on the performance of an ejector enhanced refrigeration cycle using hydrocarbon mixture R290/R600a, Appl. Therm. Eng. 164 (2020), 114456.
[17] X. She, L. Cong, B. Nie, G. Leng, H. Peng, Y.i. Chen, X. Zhang, T. Wen, H. Yang, Y. Luo, Energy-efficient and-economic technologies for air conditioning with vapor compression refrigeration: A comprehensive review, Appl. Energy 232 (2018) 157–186.
[18] M. Salem, H. El-Gammal, A. Abd-Elaziz, K. Elshazly, Study of the performance of a vapor compression refrigeration system using conically coiled tube-in-tube evaporator and condenser, Int. J. Refrig 99 (2019) 393–407.
[19] S. Zakeralhoseini, B. Sajadi, M.A.A. Behabadi, S. Azarhazin, H. Fazelnia, Experimental investigation of the heat transfer coefficient and pressure drop of R1234yf during flow condensation in helically coiled tubes, Int. J. Therm. Sci. 157 (2020), 106516.
[20] C. Zhang, D. Wang, S. Xiang, Y. Han, X. Peng, Numerical investigation of heat transfer and pressure drop in helically coiled tube with spherical corrugation, Int. J. Heat Mass Transf. 113 (2017) 332–341.
[21] L. Xie, Y. Xie, J. Yu, Phase distributions of boiling flow in helical coils in high gravity, Int. J. Heat Mass Transf. 80 (2015) 7–15.
[22] B. Hardik, S. Prabhu, Heat transfer distribution in helical coil flow boiling system, Int. J. Heat Mass Transf. 117 (2018) 710–728.
[23] B. Hardik, G. Kumar, S. Prabhu, Boiling pressure drop, local heat transfer distribution and critical heat flux in horizontal straight tubes, Int. J. Heat Mass Transf. 113 (2017) 466–481.
[24] F. Zafar, M.M. Alam, Mixed convection heat transfer from a circular cylinder submerged in wake, Int. J. Mech. Sci. 183 (2020), 105733.
[25] O. Abushammala, R. Hreiz, C. Lemaître, E. Favre, Heat and/or mass transfer intensification in helical pipes: Optimal helix geometries and comparison with alternative enhancement techniques, Chem. Eng. Sci. 234 (2021), 116452.
[26] D.G. Prabhanjan, T.J. Rennie, G.S. Vijaya Raghavan, Natural convection heat transfer from helical coiled tubes, Int. J. Therm. Sci. 43 (4) (2004) 359–365.
[27] R. Andrzejczyk, T. Muszynski, M. Gosz, Experimental investigations on heat transfer enhancement in shell coil heat exchanger with variable baffles geometry, Chem. Eng. Process.-Process Intensif. 132 (2018) 114–126.
[28] A.D. Tuncer, A. Sözen, A. Khanlari, E.Y. Gürbüz, H.İ. Variyenli, Analysis of thermal performance of an improved shell and helically coiled heat exchanger, Appl. Therm. Eng. 184 (2021) 116272.
[29] A.S. Baqir, H.B. Mahood, A.R. Kareem, Optimisation and evaluation of NTU and effectiveness of a helical coil tube heat exchanger with air injection, Therm. Sci. Eng. Prog. 14 (2019), 100420.
[30] S. Khorasani, A. Dadvand, Effect of air bubble injection on the performance of a horizontal helical shell and coiled tube heat exchanger: An experimental study, Appl. Therm. Eng. 111 (2017) 676–683.
[31] S. Khorasani, A. Moosavi, A. Dadvand, M. Hashemian, A comprehensive second law analysis of coil side air injection in the shell and coiled tube heat exchanger: An experimental study, Appl. Therm. Eng. 150 (2019) 80–87.
[32] H.S. Dizaji, S. Jafarmadar, M. Abbasalizadeh, S. Khorasani, Experiments on air bubbles injection into a vertical shell and coiled tube heat exchanger; exergy and NTU analysis, Energy Convers. Manage. 103 (2015) 973–980.
[33] A. Moosavi, M. Abbasalizadeh, H.S. Dizaji, Optimization of heat transfer and pressure drop characteristics via air bubble injection inside a shell and coiled tube heat exchanger, Exp. Therm Fluid Sci. 78 (2016) 1–9.
[34] D. Panahi, Evaluation of Nusselt number and effectiveness for a vertical shell-coiled tube heat exchanger with air bubble injection into shell side, Exp. Heat Transfer 30 (3) (2017) 179–191.
[35] S. Pourhedayat, H. Sadighi Dizaji, S. Jafarmadar, Thermal-exergetic behavior of a vertical double-tube heat exchanger with bubble injection, Exp. Heat Transfer 32 (5) (2019) 455–468.
[36] E.M. El-Said, M. Abou Alsood, Experimental investigation of air injection effect on the performance of horizontal shell and multi-tube heat exchanger with baffles, Appl. Therm. Eng. 134 (2018) 238–247.
[37] K. Ökten, A. Biyikoglu, Effect of air bubble injection on the overall heat transfer coefficient, J. Enhan. Heat Transfer 25 (3) (2018) 195–210.
[38] M.M. Heyhat, A. Abdi, A. Jafarzad, Performance evaluation and exergy analysis of a double pipe heat exchanger under air bubble injection, Appl. Therm. Eng. 143 (2018) 582–593.
[39] S.L. Ghashim, A.M. Flayh, Experimental investigation of heat transfer enhancement in heat exchanger due to air bubbles injection, J. King Saud Univ.-Eng. Sci. 33 (7) (2021) 517–524.
[40] D. Sánchez, R. Cabello, R. Llopis, I. Arauzo, J. Catalán-Gil, E. Torrella, Energy performance evaluation of R1234yf, R1234ze (E), R600a, R290 and R152a as low-GWP R134a alternatives, Int. J. Refrig 74 (2017) 269–282.
[41] J.U. Ahamed, R. Saidur, H.H. Masjuki, A review on exergy analysis of vapor compression refrigeration system, Renew. Sustain. Energy Rev. 15 (3) (2011) 1593–1600.
[42] H.B. Al Ba'ba'a, T. Elgammal, R.S. Amano, Correlations of bubble diameter and frequency for air–water system based on orifice diameter and flow rate, J. Fluids Eng. 138 (11) (2016).
[43] H. Moradi, A. Bagheri, M. Shafaee, S. Khorasani, Experimental investigation on the thermal and entropic behavior of a vertical helical tube with none-boiling upward air-water two-phase flow, Appl. Therm. Eng. 157 (2019), 113621.
[44] A. Alimoradi, Investigation of exergy efficiency in shell and helically coiled tube heat exchangers, Case Stud. Therm. Eng. 10 (2017) 1–8.
[45] A. Sheeba, C. Abhijith, M.J. Prakash, Experimental and numerical investigations on the heat transfer and flow characteristics of a helical coil heat exchanger, Int. J. Refrig 99 (2019) 490–497.
[46] C.-N. Chen, J.-T. Han, T.-C. Jen, L.i. Shao, Thermo-chemical characteristics of R134a flow boiling in helically coiled tubes at low mass flux and low pressure, Thermochim Acta 512 (1-2) (2011) 163–169.
[47] E. Izadpanah, A. Zarei, S. Akhavan, M.B. Rabiee, An experimental investigation of natural convection heat transfer from a helically coiled heat exchanger, Int. J. Refrig 93 (2018) 38–46.
[48] R.J. Moffat, Describing the uncertainties in experimental results, Exp. Therm Fluid Sci. 1 (1) (1988) 3–17.
[49] A. Bejan, Convection heat transfer, John Wiley & Sons (2013).
[50] G. Besagni, F. Inzoli, T. Ziegenhein, Two-phase bubble columns: A comprehensive review, ChemEngineering 2 (2) (2018) 13.
[51] S. Dizaji, Heat transfer enhancement due to air bubble injection into a horizontal double pipe heat exchanger, Automot. Sci. Eng. 4 (4) (2014) 902–910.